ACS APPLIED MATERIALS & INTERFACES

RESEARCH ARTICLE

www.acsami.org

Fabrication of PbS Nanoparticle-Sensitized TiO_2 Nanotube Arrays and Their Photoelectrochemical Properties

Qing Kang,[†] Shaohuan Liu,[†] Lixia Yang,[†,‡] Qingyun Cai,[*,†] and Craig A. Grimes[§]

[†]State Key Laboratory of Chemo/Biosensing and Chemometrics, Department of Chemistry, Hunan University, Changsha 410082, P. R. China

[‡]School of Environment and Chemical Engineering, Nanchang Hangkong University, Nanchang 330063, P. R. China

[§]Photonic Fuels LLC, 254 Innovation Park, State College, Pennsylvania 16803, United States

ABSTRACT: TiO_2 nanotube arrays (NTAs) are modified with PbS nanoparticles by successive ionic layer adsorption and reaction (SILAR) or electrodeposition, with an aim towards tuning the photoelectrochemical cell to the visible region. The PbS modification of the TiO_2 NTAs results in an increase in the visible light adsorption, however the increase in photocurrent is dependent on the modification method. PbS/TiO_2 NTAs prepared by SILAR and electrodeposition show, respectively, photocurrents of 11.02 and 5.72 mA/cm^2. The increase in photocurrent is attributed to enhanced charge separation efficiency and improved electron transport.

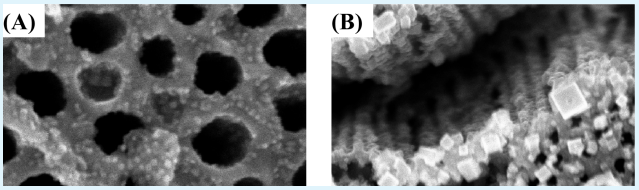

KEYWORDS: SILAR, Electrodeposition, TiO_2 nanotube, PbS, Nanoparticle, Photocurrrent

1. INTRODUCTION

Nano-dimensional titanium dioxide (TiO_2) is one of the most important wide bandgap semiconductors, widely used as a photocatalyst because of its high stability, non-toxicity, high oxidative power and low cost.[1−4] Among all the TiO_2 nanostructured materials studied in recent years, TiO_2 nanotube arrays (NTAs) prepared by electrochemical anodization of titanium have attracted great attention due to their excellent photocatalytic properties.[5,6] However, their photoelectrochemical utility is limited by its UV-responsive band gap of approximately 3.2 eV. Therefore much effort has been spent in the attempt to prepare TiO_2-based photocatalysts that efficiently adsorb in visible region. Such efforts include doping TiO_2 NTAs with metal/nonmental ions to induce a red shift to the band gap,[7−9] and coupling TiO_2 NTAs with low-band-gap semiconductors.[10−12] Among the low-band -gap semiconductors, lead sulfide (PbS) is an attractive semiconductor as its band gap is dependent on the particle size. Bulk PbS has a band gap of 0.42 eV, whereas PbS nanoparticles less than 5 nm in diameter have a band gap of 0.88 eV.[13,14] By controlling the size of the PbS nanoparticles the absorption wavelength of the first excition peak can be easily extended into the infrared. Further, with the TiO_2 NTA architecture enabling efficient spatial separation of the photogenerated charges, it is possible that suitable PbS nanoparticles could enhance TiO_2 photocatalytic activity because of multiple exciton generation.[15,16]

We seek to combine the excellent photochemical and charge transport properties of the crystalline TiO_2 NTAs with the excellent visible light absorption properties of PbS, thereby shifting the absorption characteristics of the composite material into the visible spectrum. Although there are studies focusing on the sensitization of TiO_2 with PbS,[17,18] there are few reports on the modification of these highly ordered, self-assembled TiO_2 NTAs with PbS nanoparticles for photoelectrochemical cell application. In this work, PbS nanoparticles were deposited onto the TiO_2 NTAs by using a successive ionic layer adsorption and reaction (SILAR) process, as well as electrodeposition. We evaluate charge transfer from the PbS nanoparticles to the TiO_2 NTAs, comparing the performance of the PbS-modified TiO_2 NTAs prepared by SILAR and electrodeposition within a photoelctrochemical cell.

2. EXPERIMENTAL DETAILS

2.1. Preparation and Characterization of the PbS/TiO_2 NTAs. Titanium foils (250 μm thick, 99.8%) were purchased from Aldrich (Milwaukee, WI). NH_4F, ethylene glycol (EG, 99.8%), Na_2S, CH_3OH, $Pb(NO_3)_2$, $Na_2S_2O_3$, and HNO_3 of analytic grade were purchased from commercial sources. Twice-distilled water was used throughout this experiment.

Titanium foil samples were cut into 1 × 3 cm^2 pieces ultrasonically cleaned in acetone and ethanol and then anodized in ethylene glycol containing 0.3 wt % NH_4F and 2% volume of H_2O at the constant voltage of 40 V for 2 h. The anodizing cell was a two-electrode configuration with a Pt sheet cathode and the Ti sheet as the anode. All experiments were conducted at about 25°C. The resulting amorphous titania nanotube arrays were annealed at 450°C for 2 h with heating and cooling rates of 2°C/min in an air to crystallize the nanotube walls.

Received: November 10, 2010
Accepted: January 20, 2011
Published: February 09, 2011

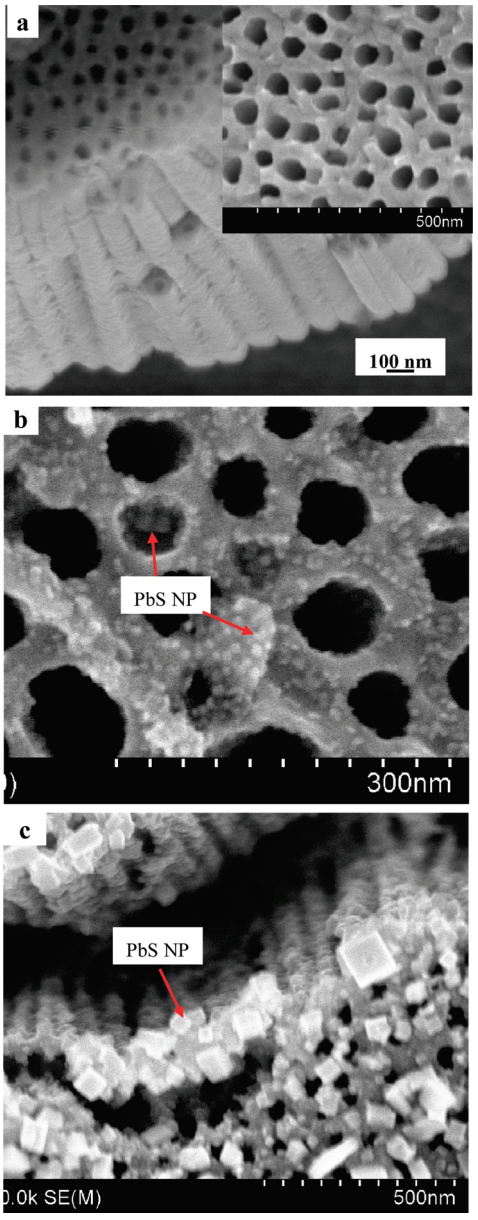

Figure 1. FE-SEM of (a) TiO_2 NTAs and (b, c) PbS/TiO_2 NTAs prepared by (b) SILAR (6 cycles) or (c) electrodeposition (1200 s).

PbS nanopatricles were deposited onto the TiO_2 NTAs by SILAR and electrodeposition. In the SILAR process the TiO_2 NTA electrode was successively immersed, 1 min for each step, in 0.001 M $Pb(NO_3)_2$ in methanol, pure methanol, 0.001 M Na_2S in methanol, and pure methanol. After a methanol wash the electrode was dried in air. This whole procedure is referred to as one full coating cycle. The TiO_2 NTA electrode became dark after several cycles because of the deposition of small PbS NPs.

The electrodeposition of PbS nanoparticles was conducted by cathodic reduction using a conventional three-electrode system with the TiO_2 sheet as the working electrode, a saturated calomel electrode (SCE) reference electrode and a Pt wire counter electrode. The electrolyte contained 1 mM $Pb(NO_3)_2$ and 1 mM $Na_2S_2O_3$. The pH was adjusted to 3 by adding a few drop of 0.5 M HNO_3. The cathodic deposition potential of PbS was chosen to be −0.65 V through cyclic voltammograms (CVs). After electrodeposition, the samples were thoroughly rinsed by twice-distilled water.

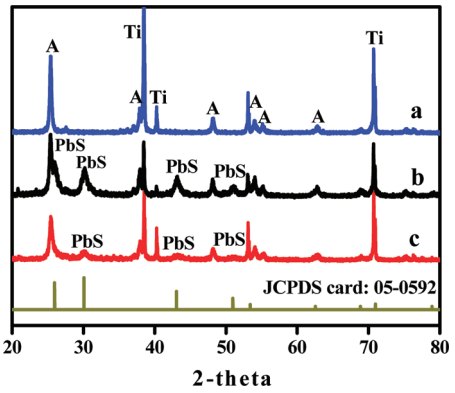

Figure 2. XRD of (a) TiO_2 NTAs and (b, c) PbS/TiO_2 NTAs prepared by (b) SILAR (18 cycles) or (c) electrodeposition (2000 s).

After PbS deposition all PbS/TiO_2 NTA electrode samples were annealed at 300°C for 1 h in nitrogen.

The topology of the prepared PbS/TiO_2 NTAs was characterized using a field-emission scanning electron microscope (FE-SEM) operating at 5 kV (Hitachi, model S-4800, Japan). Energy-dispersive X-ray (EDX) spectrometers fitted to the electron microscopes were used for elemental analysis. The crystal structure of the PbS/TiO_2 NTA samples was characterized using a X-ray diffractometer (XRD, M21X, MAC Science Ltd., Japan) with Cu Ka radiation (λ = 1.54178 Å). Absorption spectra were recorded using a UV−vis spectrophotometer (Vary 300, USA) equipped with an integrating sphere of 150 mm radius.

2.2. Photoelectrochemical Measurements. The photoelectrochemical response of the samples was measured with a CHI 600C electrochemical workstation (Shanghai, Chenhua) using a conventional three-electrode system comprising of a SCE reference electrode and a Pt wire counter electrode in 0.2 M Na_2S aqueous electrolyte. Full-spectrum illumination at an intensity of 100 mW/cm^2 was provided with a 300 W high-pressure xenon short arc lamp (PLS-SXE300, Beijing Changtuo).

2.3. Photocatalytic Degradation of Methyl Orange. Characterization of the photocatalytic degradation properties of the different (1 cm^2) samples was performed in a cubic quartz reactor containing 30 ml methyl orange (MO) solution at an initial concentration of 5×10^{-5} mol/L. The degradation cell was kept stirring in dark for 3 h to achieve an adsorption equilibrium for MO. Then the cell was exposed to simulated sunlight of 100 mW/cm^2. The change in MO concentration was monitored by determining the UV−visible adsorption of 2.0 mL sample taken from the solution every 30 min. After measurement, the sample was put back to the reaction solution to keep the volume constant.

3. RESULTS AND DISCUSSION

3.1. Characterization of the PbS/TiO_2 NTA Samples. Figure 1a shows the TiO_2 NTA morphology, with a nanotube length of about 500 nm and an average pore diameter of 60 nm. Figure 1b shows that the PbS nanoparticles prepared by SILAR (6 cycles) are ~6 nm in diameter and are distributed on both the outside and inside of the TiO_2 NTAs. Figure 1c shows that PbS nanoparticles prepared by electrodeposition at −0.65 V for 1200 s are hexahedral crystals ranging in size from 8 to 54 nm, and are distributed mainly on the top surface of the nanotubes.

Figure 2 shows the XRD spectrum of the TiO_2 NTAs before and after modification with PbS. The XRD spectrum, Figure 2a, of the unmodified TiO_2 NTAs confirms that the 450°C annealed TiO_2 NTAs are anatase. Spectra b and c in Figure 2 reveal that PbS prepared by either 18 SILAR cycles or 2000 s electrodeposition is cubic phase with the most intense peaks at 2θ = 25.941,

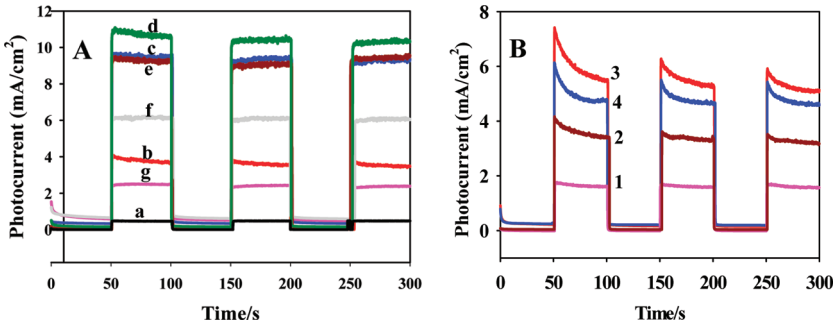

Figure 3. Current−time (I−t) measurement of PbS/TiO_2 NTAs prepared by (A) SILAR with different deposition cycles (curves a−g: 0, 1, 3, 6, 9, 15, 18 cycles), and (B) electrodeposition with different deposition times (curves 1−4: 250, 400, 500, 600s).

30.085, 43.137, and 51.030° corresponding to (111), (200), (220), and (311) planes (JCPDS file: 05-0592), respectively. The SILAR method achieves more intense XRD peaks as compared with electrodeposition. Inspection of the Figure 1 FE-SEM images reveals that the PbS particles prepared by SILAR are uniformly distributed on both the outside and inside of TiO_2 NTAs, where those prepared by electrodeposition are distributed on the top surface of the TiO_2 NTAs.

3.2. Photoelectrochemical Behavior of PbS/TiO_2 Electrodes. Photoelectrochemical (PEC) tests were carried out using the PbS/TiO_2 NTAs as the photoanode, a Pt wire cathode, and a SCE reference electrode. The current−time (I−t) characteristics of PbS/TiO_2 NTA electrodes are presented in Figure 3. The measurements were carried out in 0.2 M Na_2S electrolyte, an efficient hole scavenger for PbS. The electrodes are stable in the Na_2S solution. The photocurrent density increases first and then decreases with increasing PbS loading on both the SILAR and electrodeposition-modified electrodes. The highest photocurrent densities are achieved with the 6 SILAR cycle or 500 s electrodeposition samples. Increasing the PbS deposition time results in formation of new crystallites, and crystallite growth. As reported by Baker and co-workers,[11] large nanocrystallites are less efficient in transferring electrons than their smaller counterparts. The results of Yang et al.[14] show that with the growth of particle size the conduction band shifts lower in energy, finally approaching that of bulk PbS. Therefore, with increasing deposition time, the photocurrent first increases, with PbS sensitization of the TiO_2 surface, and then decreases as the PbS particle size continues to increase.

The PbS/TiO_2 NTAs prepared by SILAR exhibit superior performance. Figure 4 shows the UV−vis diffuse-reflectance spectra of some high performing samples; the PbS results in a red shift in the absorption edge and enhanced absorption. The PbS/TiO_2 NTAs prepared by SILAR show significantly higher absorption in the visible region, and as a result higher photocurrents, than those prepared by electrodeposition because of their uniform deposition and uniformly smaller particle size.

It is interesting to note that there is a rapid decay in the photocurrent prior to stabilization on the electrodeposited PbS/TiO_2 NTA electrode, whereas the PbS/TiO_2 NTAs prepared by SILAR show a stable photocurrent response. Larger particles are more prone to serve as electron-hole recombination centers than smaller nanoparticles.[19] Thus we believe that the higher photoelectrical efficiency of SILAR-prepared PbS/TiO_2 NTAs is partly due to the larger surface area, associated with smaller particle size and uniform coating the nanotubes, and relatively less hole-electron combination.

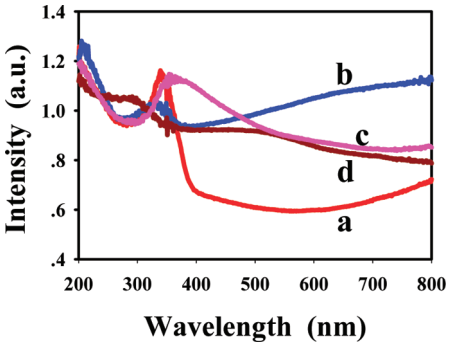

Figure 4. Diffuse reflectance absorption spectra of (a) TiO_2 NTAs; PbS/TiO_2 NTAs prepared by (b) SILAR (9 cycles) or (c) electrodeposition (600 s), and (d) PbS/Ti prepared by electrodeposition.

Figure 5 shows the current−voltage (I−V) characteristics of the PbS sensitized TiO_2 NTAs. The anodic photocurrents increase as the potential is swept toward positive values, and saturate when the potential is greater than −0.2 V (vs SCE) at which point electron transport is no longer a limiting factor. The saturated photocurrent of PbS/TiO_2 NTAs prepared by SILAR and electrodeposition reached 11.05 and 5.72 mA/cm^2, respectively. The photocurrent of the unmodified TiO_2 NTAs electrodes is negligible, indicating that PbS is a major contributor to the observed photocurrent. The open circuit potential (OCP) of the TiO_2 NTAs, PbS/TiO_2 NTAs prepared by SILAR and electrodeposition are, respectively, −0.98 V, −1.02 V and −1.13 V. As shown previously,[19,20] better charge separation and electron accumulation at the semiconductor-semiconductor interface shift the Fermi level to a more negative potential. The negative shift in the OCP is indicative of the improved energetics of the PbS/TiO_2 NTAs.

To investigate the role of TiO_2, we measured photocurrent density of the amorphous PbS/amorphous TiO_2 (A_{PbS}/A_{TiO2}) and amorphous PbS/crystalline TiO_2 (A_{PbS}/C_{TiO2}). The A_{PbS}/A_{TiO2} showed negligibly photocurrent, whereas the A_{PbS}/C_{TiO2} shows much higher photocurrent (data not shown), suggesting that crystalline TiO_2 contributes to the photocurrent response in addition to working as the template.

3.3. Photocatalytic Behavior of PbS/TiO_2 NTA Electrodes. Figure 6 shows the photocatalytic degradation of methyl orange (MO) under the influence of the unmodified TiO_2 NTA electrode and PbS/TiO_2 NTA electrode. Figure 6a is due to direct photolysis in the absence of photocatalysts. After 4 h illumination, the degradation efficiency of MO with TiO_2 NTAs, SILAR-prepared PbS/TiO_2 NTAs, and electrodeposition-prepared PbS/TiO_2

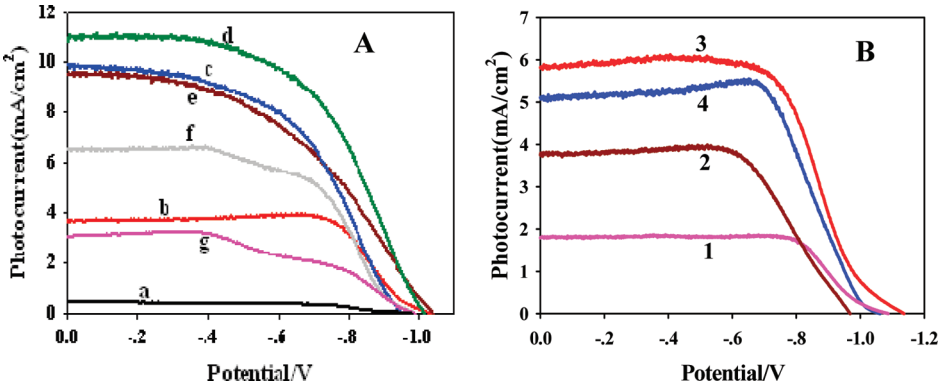

Figure 5. *I*−*V* measurement of PbS/TiO_2 NTAs prepared by (A) SILAR with different deposition cycles (curves a−g: 0, 1, 3, 6, 9, 15, 18 cycles) and (B) electrodeposition with different deposition time (curves 1−4: 250, 400, 500, 600s).

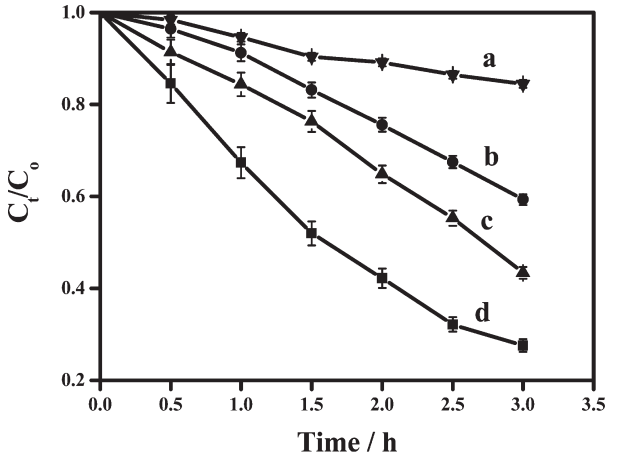

Figure 6. (a) Direct photolysis degradation, and (b−d) photocatalytic degradation of 5×10^{-5} mol L^{-1} MO (30 mL) with (b) TiO_2 NTAs and (c, d) PbS TiO_2 NTAs prepared by (c) electrodeposition or (d) SILAR.

NTAs are, respectively, 41.7, 72.44, and 56.44%. PbS plays an important role in promoting charge separation in a PbS/TiO_2 NTA heterojunction, yielding an increasing degradation rate.

4. CONCLUSIONS

The photoelectric catalytic performance of PbS/TiO_2 NTAs prepared by SILAR and electrodeposition were investigated. The sensitization of the TiO_2 nanotube arrays by the PbS nanoparticles significantly enhances the visible light response of the electrodes. The PbS/TiO_2 NTA prepared by SILAR shows higher photocurrents, and consequently higher photoelectrochemical activity. The significantly larger PbS particles produced by electrodeposition may block the TiO_2 NTAs and serve as electron-hole recombination centers in turn limiting the performance of such electrodes.

AUTHOR INFORMATION

Corresponding Author

*E-mail: qycai0001@hnu.cn.

REFERENCES

(1) Teramura, K.; Maeda, K.; Saito, T.; Takata, T.; Saito, N.; Inoue, Y.; Domen, K. *J. Phys. Chem. B* **2006**, *110*, 4500–4501.

(2) Wilson, J. M.; Idriss, H. *J. Am. Chem. Soc.* **2002**, *124*, 11284–11285.

(3) Li, X. Z.; Liu, H. L.; Yue, P. T.; Sun, Y. P. *Environ. Sci. Technol.* **2000**, *34*, 4401–4406.

(4) Li, X. Z.; Liu, H. S. *Environ. Sci. Technol.* **2005**, *39*, 4614–4620.

(5) Grimes, C. A.; Mor, G. K. . *Properties and Applications*; Springer: Norwell, MA, 2009.

(6) Shankar, K.; Basham, J. I.; Allam, N. K.; Varghese, O. K.; Mor, G. K.; Feng, X. J.; Paulose, M.; Seabold, J. A.; Choi, K. S.; Grimes, C. A. *J. Phys. Chem. C* **2009**, *113*, 6327.

(7) Cui, X. L.; Ma, M.; Zhang, W.; Yang, Y. H.; Zhang, Z. J. *Electrochem. Commun.* **2008**, *10*, 367–371.

(8) Ashai, R.; Morokawa, T.; Ohwaki, T.; Taga, Y. *Science* **2001**, *293*, 269–271.

(9) Shankar, K.; Paulose, M.; Mor, G. K.; Varghese, O. K.; Grimes, C. A. *J. Phys. D: Appl. Phys.* **2005**, *38*, 3543–3549.

(10) Chen, S.; Paulose, M.; Ruan, C.; Mor, G. K.; Varghese, O. K.; Kouzoudis, D.; Grimes, C. A. *J. Photochem. Photobiol. A* **2006**, *177*, 177–184.

(11) Baker, D. R.; Kamat, P. V. *Adv. Funct. Mater.* **2009**, *19*, 805–811.

(12) Seabold, J. A.; Shankar, K.; Wilke, R. H. T.; Paulose, M.; Varghese, O. K.; Grimes, C. A.; Choi, K. S. *Chem. Mater.* **2008**, *20*, 5266–5273.

(13) Park, J. P.; Kim, S. K.; Park, J. Y.; Ahn, S.; Ok, K. M.; Kwak, H. Y.; Shim, I. W. *Thin Solid Films* **2009**, *517*, 6663–6665.

(14) Yang, S. M.; Wang, Z. S.; Huang, C. H. *Synth. Met.* **2001**, *123*, 267–272.

(15) Brahimi, R.; Bessekhouad, Y.; Bouguelia, A.; Trari, M. *J. Photochem. Photobiol. A* **2008**, *194*, 173–180.

(16) Hyun, B. R.; Zhong, Y. W.; Bartnil, A. C. *ACS Nano* **2008**, *2*, 2206–2212.

(17) Ratanatawanate, C.; Tao, Y.; Balkus, K. J. *J. Phys. Chem. C* **2009**, *113*, 10755–10760.

(18) Ratanatawanate, C.; Xiong, C.; Balkus, K. J. *ACS Nano* **2008**, *2*, 1682–1688.

(19) Yang, L. X.; Luo, S. L.; Liu, R. H.; Cai, Q. Y.; Xiao, Y.; Liu, S. H.; Su, F.; Wen, L. F. *J. Phys. Chem. C* **2010**, *114*, 4783–4789.

(20) Kang, Q.; Lu, Q. Z.; Liu, S. H.; Yang, L. X.; Wen, L. F.; Luo, S. L.; Cai, Q. Y. *Biomaterials* **2010**, *31*, 3317–3326.